Dalton Transactions

ROYAL SOCIETY OF CHEMISTRY

PAPER

View Article Online
View Journal | View Issue



Cite this: *Dalton Trans.*, 2020, **49**, 8367

# A dinuclear rhenium complex in the electrochemically driven homogeneous and heterogeneous $H^+/CO_2$-reduction†

Lucas A. Paul,[a] Sheida Rajabi,[a] Christian Jooss,[b,c] Franc Meyer,[a,c] Fatemeh Ebrahimi[b] and Inke Siewert*[a,c]

A dinuclear $Re(CO)_3$ complex with a proton responsive phenol unit and a pyrene anchor in the ligand backbone was investigated in the electrochemical $CO_2/H^+$ conversion in solution and adsorbed on multi walled carbon nanotubes (MWCNT) on an GC electrode surface. The pyrene group unit is introduced at the end of the ligand synthesis *via* a coupling reaction, which allows for a versatile ligand modification in order to tune the electronic properties or to introduce various anchor groups for heterogenisation at a late stage. The redox chemistry of the pyrene-α-diimine-$Re(CO)_3$ complex, **1**, was investigated in *N*,*N*-dimethylformamide (dmf), including IR-spectroelectrochemical (IR-SEC) characterisation of the short lived, reduced species. Subsequently, the electrochemical $H^+/CO_2$-reduction catalysis in dmf/water was investigated. The complex catalyses syngas formation yielding CO and $H_2$ with similar rates, namely in Faraday yields of 45% and 35%, respectively. Since the similar complex without the pyrene anchor in the backbone, **I**, prefers $CO_2$ over $H^+$ reduction, the formation of syngas was rationalised by the small differences in the redox properties and p$K_a$ values of the phenol-pyrene unit in regard to phenol unit as in **I**. Subsequently, the complex was adsorbed on multi walled carbon nanotubes (MWCNT) on a GC electrode surface. Scanning electron microscopy (SEM) and X-ray photoelectron spectroscopy (XPS) confirmed coating of the electrode. The immobilised complex was utilised in the electrochemical $CO_2/H^+$ reduction in dmf/water, however, the complex quickly desorbed under reductive conditions, likely due to the good solubility of the reduced species. Water as a solvent prevents desorption as confirmed by XPS, however, then a preference for $H_2$ formation over syngas formation was observed under electrocatalytic conditions. Thus, these experiments show, that the results obtained in aqueous organic solution are not easily transferable to the heterogeneous systems operating in water due to changes in the reaction rates for competing pathways.

Received 2nd February 2020,
Accepted 3rd June 2020

DOI: 10.1039/d0dt00381f

rsc.li/dalton



## Introduction

Electrochemical $CO_2$ reduction as an alternative access to CO has been investigated intensively in the last few decades. Currently, CO is formed mainly *via* burning of fossil fuels and subsequent water gas shift reaction. The electrochemical reduction of $CO_2$ represents an appealing alternative, green approach to synthetic fuels.[1] The $2e^-/2H^+$ reduction of $CO_2$ exhibits a potential of −0.73 V *vs.* $Fc^{+/0}$ in dmf, however, it competes with the thermodynamically favoured proton reduction (−0.66 V).[2] Concomitant electrochemical CO and $H_2$ formation, *e.g.* similar reaction rates for both reaction pathways, leads to the formation of syngas, which represents a crucial intermediate in chemical industry for the synthesis of bulk chemicals. Currently syngas is mainly produced by natural gas, coal, and steam reforming, which is very redox inefficient as reduced carbonic material is oxidised and subsequently reduced again to yield, *e.g.* methanol. Thus, alternative pathways are highly desirable.

A well-known catalysts family mediating the electrochemical $CO_2$-to-CO transformation are the α-diimine-$Re(CO)_3$ complexes, which were introduced already in 1984 by Lehn and coworkers and were shown to catalyse selectively the electrochemical $CO_2$-to-CO reduction.[3] Investigation of the reaction

[a]*Universität Göttingen, Institut für Anorganische Chemie, Tammannstr. 4, 37077 Göttingen, Germany. E-mail: inke.siewert@chemie.uni-goettingen.de*
[b]*Universität Göttingen, Institut für Materialphysik, Friedrich-Hund-Platz 1, 37077 Göttingen, Germany*
[c]*Universität Göttingen, International Center for Advanced Studies of Energy Conversion (ICASEC), Tammannstr. 6, 37077 Göttingen, Germany*

†Electronic supplementary information (ESI) available. CCDC 1973247. For ESI and crystallographic data in CIF or other electronic format see DOI: 10.1039/d0dt00381f

led to a basic understanding of the mechanism.[4] Catalysis can proceed *via* the slow one electron route, in which the singly reduced species reacts after chloride loss with $CO_2$. Subsequently, the reduced Re–$CO_2$ adduct reacts with a second equivalent of $CO_2$ and a second equivalent of the reduced Re species forming a dimer. The disproportionation of the dimer leads to the re-formation of the catalyst and formation of the products CO and carbonate. In the faster two-electrons pathway, the doubly reduced species reacts after chloride ligand loss with $CO_2$. Protonation of the Re–$CO_2$ intermediate initiates C–O bond cleavage. Reduction of the tetracarbonyl species leads to CO release and regeneration of the active species. The protonation induced CO bond cleavage step in the two-electrons pathway prompted others and us to investigate the impact of a proton relay in such $Re(CO)_3$ complexes on the reactivity (Fig. 1).[5]

The introduction of a phenol unit as in **II** led, indeed, to a lower overpotential in the electrochemical $CO_2$ reduction.[5d] However, the maximum observed rate constant for catalysis was lower with **II** than for the complex with an anisole unit, since an irreversible O–H bond breaking step competes with catalysis. The complex releases $H_2$ and $Cl^-$ after reduction in a competitive pathway forming a phenolate unit, which binds to the metal centre and blocks it for $CO_2$ binding. However, the dinuclear complex **I** exhibits superior catalytic activity over Lehn's complex and **II**. It exhibits a much higher reaction rate and the same overpotential in comparison to **II**.[5d]

Some effort has been made to immobilise α-diimine-Re$(CO)_3$ complexes on electrode surfaces. Such materials can then be used as devices in the $CO_2$-to-CO reduction catalysis. One of the earliest reports for α-diimine-Re$(CO)_3$ complexes exploiting this strategy appeared in 1989.[4c] Meyer and co-workers electropolymerized (vbpy)Re$(CO)_3$ on a GC electrode (vbpy = 4-methyl-4′-vinyl-2,2′-bipyridine) and the material was moderately active in the electrochemical $CO_2$ conversion in acetonitrile. A similar approach has been pursued with redox-active thiophene units in the backbone.[6] Recently, a different strategy has been investigated: pyrene groups, which undergo π-interactions with carbonic materials, have been introduced in the ligand backbone in order to adsorb the catalyst onto the surface of carbon black[7] or edge-plane graphite[8] electrodes. The modified carbon black material was moderately active in MeCN with a faradaic yield of 70% for CO.[7] Immobilized catalysts on carbonous materials offer the advantage to use water, in which α-diimine-Re$(CO)_3$ complexes are usually not soluble, instead of organic solvents.[8,9] Warren and co-workers showed that such modified electrodes are active for $CO_2$-to-CO reduction in water and exhibit high TON.[8] This was rather unexpected as the complexes were inactive in organic solvent mixtures and thus, the heterogenisation turned an inactive complex into an active catalysts. These results prompted us to investigate the immobilisation of the dinuclear Re complex with a proton responsive ligand *via* a pyrene group in the ligand backbone, since the complex exhibits an enhanced catalytic rate for the $CO_2$-to-CO conversion with regard to Lehn's complex,[5d] and forms $H_2$ in a competitive side reaction to give valuable CO/$H_2$ (syngas) mixtures.

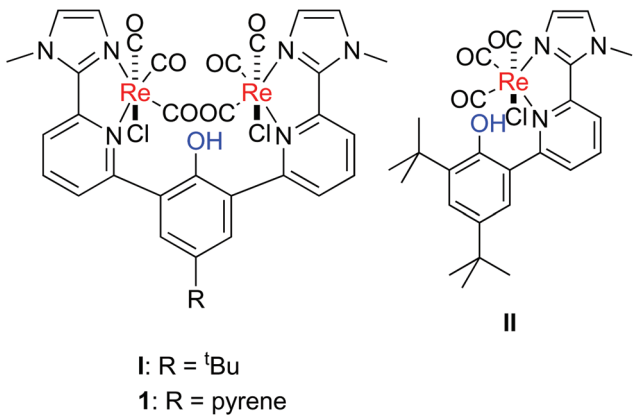


Fig. 1 Selected $Re(CO)_3$ complexes with proton responsive units, which have been used in the electrochemical $CO_2$-to-CO conversion.[5d]

## Results and discussion

### Complex synthesis and characterisation

The ligand was synthesised in a ten step procedure similar to the one described for **I**. The pyrene group was introduced in the second to the last step in a coupling reaction between the boronic acid pyrene group and the ligand precursor with a bromo function in the backbone. This allows for minimum modification of the ligand synthesis[10] and maximum flexibility in the anchor group as it is introduced late in the synthesis. The pyridine-imidazole sidearm was prepared in a Negishi coupling reaction as described previously.[10] As second building block, 2,6-diiodophenol was used. The phenol unit was protected with ethoxymethyl, converted in a Miyaura-borylation reaction with bis(pinacolato)diboron to yield the pinacolboryl derivative, and subsequently coupled with the sidearm to form the protected ligand precursor (Scheme S1†). Subsequently, the phenol was deprotected and the reaction with bromine in pyridine, which serves as a solvent and base, led to selective bromination in the 4-position of the phenol unit. Protection with ethoxymethyl was necessary prior to the coupling of the two subunits, *i.e.* the pyrene and the ligand precursor. The pyrene group was finally introduced in a Suzuki coupling reaction and the ligand was obtained after deprotection in diluted HCl solution. The ligand was fully characterised by the usual methods.

The reaction of the ligand L with $Re(CO)_5Cl$ in toluene at elevated temperature led to the formation of the desired complex $[Re_2(CO)_6(L)Cl_2]$, **1**. The IR spectrum exhibits the typical CO vibrations as expected for a facial tricarbonyl complex[11] and the frequencies are very similar to those of the parent complex **I**,[5d] which indicates that the pyrene anchor has only very little influence on the electronic structure at the Re centres. Microanalysis proved the purity of the material. Single crystals suitable for X-ray diffraction were obtained by

diffusion of diethyl ether into a saturated solution of **1** in dmf. The result of the refinement is depicted in Fig. 2, Table 1, Fig. S1 and Tables S1, S2.† As expected from IR spectroscopy, the three carbonyl ligands occupy one face of the octahedron. The pyridine units and the phenol unit are highly twisted as previously observed in **I** (Table S2†).[5b] The distance between the Re atoms and the N donor atoms are similar to the respective distances in the corresponding mono and dinuclear Re complexes **I** and **II**,[5b,d] and the same holds for the other structural parameters (Table 1). In the crystal structure two pyrene groups interact *via* $\pi$-stacking, which leads to a dimeric structure of **1** in the solid state.[12] The distance between the parallel planes defined by the pyrene groups is 3.52 Å.

In dmf-$d_7$, however, the monomer is present as determined by diffusion ordered NMR spectroscopy. The diffusion coefficient of **1** is the same as the one of **I** (*cf.* **1**: $D = 3.2 \times 10^{-10}$ m $s^{-1}$ and **I**: $D = 3.2 \times 10^{-10}$ m $s^{-1}$ in dmf-$d_7$). As in **I** and **II**, isomers of **1** exist in solution as confirmed by $^1$H NMR spectroscopy. Once the OH group points to the CO ligand and once to the chlorido ligand establishing a hydrogen bond (Scheme S2†), which leads to two sets of signals in the proton NMR spectrum (Fig. S35†). The isomer ratio of the two subunits in dmf-$d_7$ is around ~4 : 1, which is slightly different than in **I** (*cf.* 2 : 1 in dmf-$d_7$).

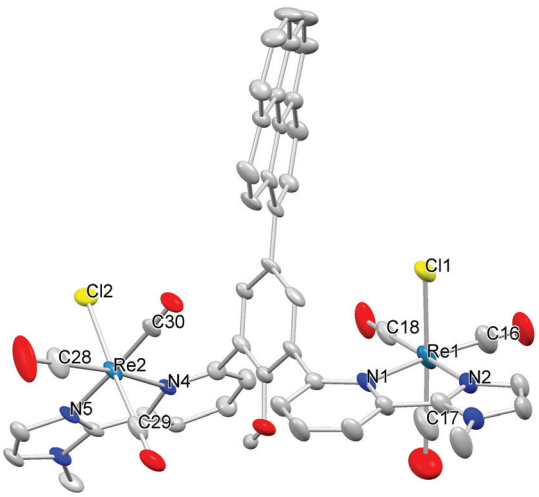


**Fig. 2** Molecular structure of **1**. Most hydrogen atoms were omitted for clarity. Thermal ellipsoids were set at the 50% level.

**Table 1** Selected bond lengths of **1**/Å

| Atoms | Distance | Atoms | Distance |
|---|---|---|---|
| Re1–N1 | 2.255(4) | Re2–N5 | 2.135(3) |
| Re1–N2 | 2.134(3) | Re2–N4 | 2.233(4) |
| Re1–Cl1 | 2.475(2) | Re2–Cl2 | 2.482(1) |
| Re1–C16 | 1.897(6) | Re2–C28 | 1.906(6) |
| Re1–C17 | 1.900(7) | Re2–C29 | 1.911(5) |
| Re1–C18 | 1.941(5) | Re2–C30 | 1.918(4) |

## Electrochemical characterisation in solution

We utilised a GC working electrode and a Pt counter electrode for the measurements. All cyclic voltammetry (CV) data in organic solvent (mixtures) were referenced internally *vs.* the redox couple of ferrocene ($Fc^{+/0}$) and data in water *vs.* the saturated calomel electrode (SCE).[13] The CV data of **1** in dmf show four reduction waves at $E_{p,c,1} = -2.10$ V, $E_{p,c,2} = -2.35$ V, $E_{p,c,3} = -2.46$ V, and $E_{p,c,4} = -2.70$ V, $\nu = 0.1$ V $s^{-1}$ (Fig. 3 and Fig. S2†). In the reverse scan, four re-oxidation waves appear at $E_{p,a,1} = -1.90$ V, $E_{p,a,2} = -2.12$ V, $E_{p,a,3} = -2.40$ V, and $E_{p,a,4} = -2.56$ V. With increasing scan rate, the CV data change, which indicates that the reduction processes are coupled to chemical reactions (Fig. S2†). At scan rates of 1 V $s^{-1}$, the first wave becomes slightly reversible, that is a re-oxidation wave appears, and a further redox process at $E_{p,a} = -2.20$ V appears. The second process $E_{p,c,2}$ at −2.35 V shifts with increasing scan rates, $E_{p,a,3}$ becomes more prominent and shifts to −2.52 V. The process at −2.70 V does not shift and remains reversible. The peak potentials of the first three processes are very similar to the ones in **I** indicating similar reduction chemistry of **1** and **I** and only minor influences of the anchor group (Fig. S3†). However, the redox process at $E_{p,c,4}$ at −2.70 V is not present in the CV data of **I** and thus, it likely belongs to the reduction of pyrene. Pyrene exhibits a reduction process at −2.60 V in acetonitrile.[14,15] The appearance of further reduction waves with increasing scan rates indicates chemical reactions such as chloride dissociation or OH bond cleavage following the reduction processes. Similar observations were made previously for **I** and **II**.[5b,d] Thus, IR-SEC experiments were pursued to identify the reduced species.

Initial reduction leads to the formation of a species $\mathbf{1^A}$, which exhibits CO absorption frequencies that are only slightly shifted with regard to **1** (Fig. 4, Table 2). The small shift indicates a reductive O–H bond cleavage, formation of 0.5 equiv. of $H_2$ and chloride ion loss as observed previously in **I** and similar complexes (Scheme S3†).[5a–d] Thus the overall process

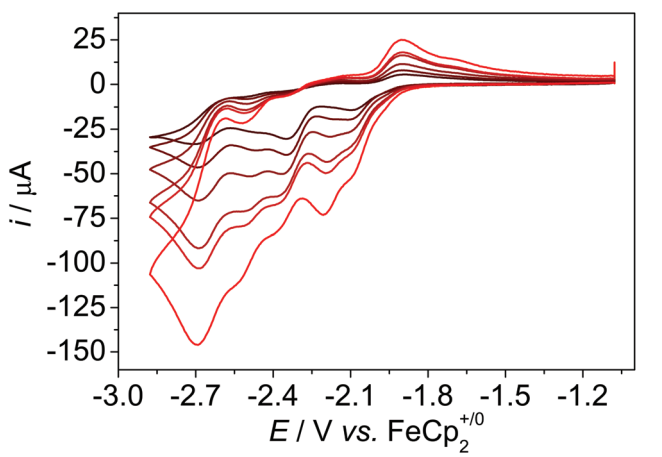


**Fig. 3** Scan rate dependent CV data of **1** under $N_2$ atmosphere, dmf, c = 1 mM, 0.1 M $^n$Bu$_4$NPF$_6$, $\nu$ = 0.1, 0.2, 0.4, 0.8, 1, 2 V $s^{-1}$. Further potential ranges can be found in Fig. S2.†

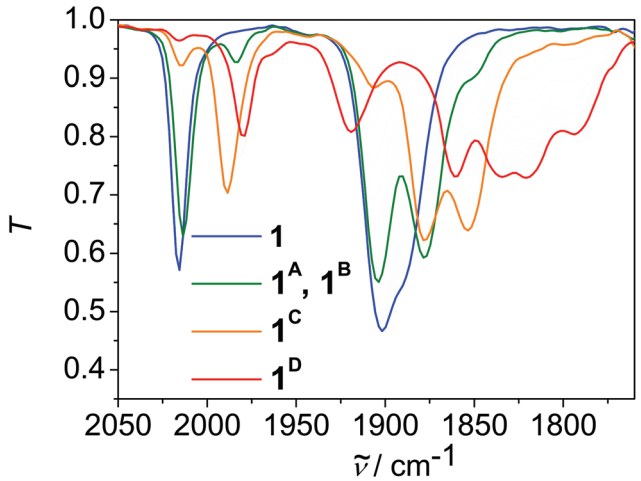


Fig. 4 Linear sweep IR-SEC of **1** in dmf, 0.1 M $^{n}Bu_4NPF_6$.

Table 2 IR Stretching frequencies of the CO bands in **1** during reduction in dmf, 0.1 M $^{n}Bu_4NPF_6$. $LH_{-1}$ denotes the ligand, which is deprotonated at the phenol unit forming a phenolate unit

| | $\nu$(CO)/cm$^{-1}$ | Tentative assignment |
|---|---|---|
| **1** | 2015, 1901, 1889 | **1** |
| $\mathbf{1^A}$ | 2012, 1903, 1878 | $[Re_2(CO)_6(LH_{-1})Cl]$ |
| $\mathbf{1^B}$ | 1984, 1850[a] | $\{Re(CO)_3L\}$-entity |
| $\mathbf{1^C}$ | 1988, 1878, 1852 | $[Re_2(CO)_6(LH_{-1})Cl]^{2-}$ |
| $\mathbf{1^D}$ | 1980, 1918, 1860, 1835, 1819, 1793 | $[Re_2(CO)_6(LH_{-1})]^{2-}$ |

[a] Further bands are masked by the main species.

is redox neutral for the complex and the net reaction for **1** represents HCl elimination. Indeed, the reaction of **1** with LDA led to a species, which exhibits CO absorption frequencies at the same frequencies as $\mathbf{1^A}$, which supports this assignment (Fig. S28†). We assume that phenolate binds to the metal centre as the CO stretching frequencies of $\mathbf{1^A}$ are typical for facial tricarbonyl rhenium complexes with a X-type ligand in trans position to one CO ligand, that are chloride and phenolate, respectively. In parallel, a further species $\mathbf{1^B}$ appears in small amounts, which exhibits CO absorption frequencies shifted in average by −35 cm$^{-1}$ with regard to **1**, which indicates the formation of a complex with a $\{Re(CO)_3L\}$-entity, that is one entity in the complex is reduced and the chlorido ligand is ejected.[16] These two parallel reaction pathways have been observed previously in **II**.[5d] Since chloride ion loss is a reversible reaction whereas OH bond cleavage and $H_2$ formation is an irreversible step, **1** is converted to $\mathbf{1^A}$ over time.

Further reduction of **1** leads to a species $\mathbf{1^C}$ with three CO vibrations, which are shifted in average by about −25 cm$^{-1}$ with regard to $\mathbf{1^A}$. This indicates the formation of a species, in which each diimine-ligand entity is reduced once and each $Re^I$ ion is coordinated by one X-type ligand, that is chloride and phenolate, respectively. Further reduction leads to the final species $\mathbf{1^D}$, which exhibits 6 CO absorption frequencies indicating the formation of an asymmetric species. Likely this is the threefold reduced species $[Re_2(CO)_6(LH_{-1})]^{2-}$ in which one Re entity is reduced twice, one Re entity once, and both chlorido ligands are dissociated (Scheme S3†). We assume that the reduction equivalents are localised on one Re-unit on the time scale of the IR, since the ligand is highly twisted.

### $CO_2$ reduction catalysis in solution

Prior to anchoring of the complex, we investigated the catalytic activity of **1** in solution. Purging a solution of **1** in dmf with $CO_2$, led to an increased current, which is indicative for a catalytic event (Fig. 5). In the presence of 6% or 10% of water, the current increase is less prominent, however, the onset potential of the catalysis is shifted to higher potentials. No current increase is observed, when water is added under argon atmosphere (Fig. S4†). Since dmf/water exhibits a pH of about 10, which decreases upon purging with $CO_2$, these experiments indicate that the catalytic event is connected to $H^+/CO_2$ reduction catalysis under less basic conditions.

Controlled potential electrolysis (CPE) experiments at an applied potential of −2.20 V in dmf + 10% water led to the formation of CO and $H_2$ in Faraday efficiencies (FE) of 45% and 35%, respectively (Table S3†). The charge builds up steadily over the course of the electrolysis experiment, which indicates good stability of **1** under catalytic conditions (Fig. S23†). The amount of $H_2$ formed is much larger than in the experiments with **I** and **II**,[5b,d] which indicates that **1** catalyses the CO and $H_2$ evolution reaction in competitive reaction pathways with similar rates. The applied potential has only minor influence on the rates of $H_2$ and CO formation, though larger non-productive currents arise under more reductive conditions (Fig. S24†). CPE experiments at an applied potential of −2.50 V led to the formation of CO and $H_2$ in Faraday efficiencies (FE) of 30% and 20%, respectively (Table S3†). Since the redox chemistry of **1** and **I** is very similar up to the applied potential of the catalysis (Fig. S3†), we hypothesize that this could be rationalised by different H-bonding properties, p$K_a$ values and OH bond dissociation free energies (BDFE) in **1** and **I** due to

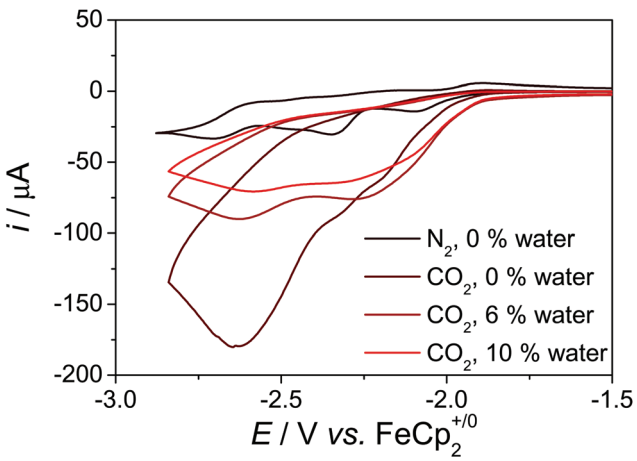


Fig. 5 CV data of **1** the presence and absence of $CO_2$ in dmf with various amounts of water, $c$ = 1 mM, 0.1 M $^{n}Bu_4NPF_6$, $\nu$ = 0.1 V s$^{-1}$.

the conjugated pyrene anchor. The H-bonding properties of the phenol OH proton in **1** and **I** are different as reflected by the $^1$H resonance of the OH-proton in dmso,[17] which is shifted downfield in **1** in comparison to **I** (**1**: *cf.* $\delta$ = 9.79 and 9.17 ppm (dmso-$d_6$) (Fig. S35†), 10.39 and 9.25 ppm (dmf-$d_7$); **I**: $\delta$ = 9.11 and 8.57 ppm (dmso-$d_6$)[5b] and 9.71 and 8.79 (dmf-$d_7$)). Furthermore, the p$K_a$ of the phenol in **1** should be lower than in **I** due the extended π-system in 4 position as this increases the stability of the anion, *i.e.* **1** is more acidic than **I**. Since pyrene, which is in conjugation with the phenol, exhibits a reduction process at −2.60 V and an oxidation process at 0.93 V,[14] the BDFE of the reduced and protonated[5a] as well as the oxidised phenol-pyrene unit in **1** should be slightly different in comparison to 2,4,6-tri-*tert*-butyl-phenol (*cf.* oxidation of phenol in dmso: 1.00 V (ref. 18)). Assuming free energy relationships for the $H_2$ formation pathways in **1** and **I**, these small differences may lead to different reaction rates for $H_2$ formation.

Scan rate dependent CV data showed, that the catalytic waves do not exhibit an S-shape, that the currents are not fully scan rate independent, and that all CVs have a wave at the foot of the catalytic wave (Fig. S5–S7†). Thus, the catalytic rate constant $k_{obs}$ can only be estimated from the limiting current according to eqn (1).[19] Dividing $i_{cat}$ (catalytic current) by $i_p$ (current of a non-catalytic event) eliminates several constants (eqn (2)).[20] The plots of $i_{cat}/i_p$ *vs.* $\nu^{-1/2}$ gave straight lines with reasonable intercepts (Fig. S8–S10†). $i_p$ was estimated from the first reduction process in the scan rate dependent CV data of **1** in the presence of LDA as this process represents a reversible 1 $e^-$ reduction event (Fig. S11†).

$$i_{cat} = n_{cat} \cdot F \cdot A \cdot C_{cat} \cdot \sqrt{D_{cat} \cdot k_{obs}} \quad (1)$$

$$\frac{i_{cat}}{i_p} = 2.242 \cdot n_{cat} \sqrt{\frac{R \cdot T}{n_p^3 \cdot F}} \sqrt{k_{obs}} \sqrt{\frac{1}{\nu}} \quad (2)$$

$n$ = number of transferred electrons, *i.e.* 2 for $H^+$ and $CO_2$ reduction, $R$ = gas constant, $T$ = temperature, $F$ = Faraday constant, $\nu$ = scan rate; $k_{obs}$ = observed catalytic rate constant (Table 3).

The overpotentials $\eta$ were estimated from the half-peak potentials of the catalytic waves.[21] The $CO_2|CO$ reduction potential is −0.73 V (ref. 2) and the $H^+|H_2$ reduction potential is −0.66 V (ref. 2 and 13) in dmf. The $CO_2|CO$ reduction potential in dmf/water has been determined to be −1.4 ± 0.1 V and the $H^+|H_2$ reduction potential is also −1.38 V based on the p$K_a$ value of 12.2 ± 1 for $H_2CO_3$ in dmf.[22]

In the presence of water, the half peak potential of the catalytic waves of **I** and **1** are the same, and less negative than in the absence of water, however, the rate constant with **1** is lower than with **I**.[5b] In the absence of water, the rate constant is higher in **1** than in **I**, though, the overpotential is higher. The lower overpotential of **1** in the presence of water may be rationalised – as previously for **I** and **II** – by the faster chloride ion loss in the protic environment due to better stabilisation of the anion.[5d] Chloride loss represents the first step in the catalytic cycle. However, the overall catalytic rate constant is smaller in **1** than in **I**, which can be rationalised by the OH-bond breaking reaction, which is considerably faster in **1** than in **I**.[5b] Only traces of $H_2$ were observed with **I**, while considerable amounts of $H_2$ were formed in the presence of **1** (*vide infra*). OH bond breaking results in the formation of the anionic rhenium species in which the 6$^{th}$ coordination side is blocked by the phenolate (*vide supra*, formation of $\mathbf{1^A}$). Further protonation re-forms the starting material.

Table 3 Key catalysis parameter of **1**; potentials at $\nu$ = 0.1 V $s^{-1}$, $k_{obs}$ from the slope of the $i_{cat}/i_p$ *vs.* $\nu^{-1/2}$ plots, $c_1$ = 1 mM, 0.1 M $^nBu_4NPF_6$, dmf, $CO_2$ atmosphere

| | 0% $H_2O$ | | | |
|---|---|---|---|---|
| | 1. wave | 2. wave | 6% $H_2O$ | 10% $H_2O$ |
| $E_{cat}{}^{1/2}$/V | −2.13 | n. d.[a] | −2.06 | −2.06 |
| $\eta$/V | 1.4 | n. d.[a] | 0.7 | 0.7 |
| $k_{obs}/s^{-1}$ | 6.5 | 12 | 9 | 8 |

[a] The potentials could not be determined, see Fig. S5.†

### Anchoring of the complex on MWCNT

Subsequently, we anchored the complex on multi-walled carbon nanotubes (MWCNT). Pre-treated MWCNTs (1 mg $mL^{-1}$) were suspended in thf and the suspension was dip coated several times on GC electrodes. Scanning electron microscopy (SEM) pictures of the GC electrode surface showed that the electrode surface was covered successfully with carbon nanotubes (Fig. S29†). Subsequently, the electrode was soaked in a saturated acetonitrile solution of **1** overnight. SEM pictures indicate that this does not change the surface morphology, and the carbon nanotubes are still present (Fig. S30†). High resolution XPS of the electrode surface confirmed the adsorption of the complex on the surface as the rhenium $4f^{7/2}$ and $4f^{5/2}$ peaks were present at 41.6 eV and 43.8 eV, respectively, which is characteristic for an α-diimine-$Re(CO)_3Cl$ complex (Fig. S32†).[7]

Electrochemical measurements of **1**@MWCNT have initially been conducted in dmf/water mixtures 10/1. CV measurements of **1**@MWCNT showed two reduction processes with peak potentials $E_{p,c}$ at ∼−1.97 V and at ∼−2.57 V ($\nu$ = 0.1 V $s^{-1}$, Fig. S12†). The catalyst loading was estimated from the first scan under $N_2$. Assuming that the first redox wave in **1**@MWCNT belongs to a 2 electrons reduction process as it does for **1** in solution (*vide supra*), we estimated a catalyst loading of $8 \times 10^{-13}$ mol on the electrode surface from the charge injected in the first wave ($Q = 1.5 \times 10^{-7}$ C, $\varnothing_{geometric}$ = 3 mm, Fig. S13†). The potential of the initial reduction of **1** shifted to slightly higher potentials with regard to solution, likely due to the differences in the solvation free energies and ion paring of a surface bound species *vs.* solution species.[23] However, the current decreases quickly with increasing number of cycles and the redox waves of **1** disappear, indicating that the catalyst is detached upon successive reductive scanning (Fig. S12†). Blank measurements show that the current also decreases with increasing cycles in the absence of

**1** due to smaller capacitive currents (Fig. S17†). However, the currents of the first scans of bare MWCNT are lower than of **1**@MWCNT and thus, the decrease in **1**@MWCNT cannot be related only to changes in the capacitive currents.

Using a freshly prepared sample and purging the solution with $CO_2$ leads to an increased current with regard to the $N_2$ measurement with two distinct plateaus at around −2.25 V and around −2.55 V (Fig. 6 and Fig. S14†). However, as under $N_2$ atmosphere, the current decreases upon successive cycling and reaches the current as under $N_2$ at the ~15$^{th}$ cycle (Fig. S15 and S16). In the CV experiment with bare MWCNT under $CO_2$ atmosphere, the current in the CV is not larger than the current in the CV experiments under $N_2$, and the absolute current is lower than in the experiments with **1**@MWCNT (Fig. S17†). These results suggest that the catalyst is not bound strongly to the surface under reductive conditions and dissolves in dmf/water. This was substantiated in a CPE experiment at an applied potential of −2.20 V for 30 minutes: the current decreases quickly within the first 50 seconds, indicating a rapid loss of activity of the hybrid (Fig. S25†). Indeed, XPS measurements of the electrode surface after electrolysis with **1**@MWCNT showed the absence of rhenium atoms, which confirms the hypothesis that the catalyst dissolves under catalytic conditions (Fig. S33†). SEM pictures of the electrode surface after extended electrolysis, however, showed that the MWCNT are still present (Fig. S31†). This means that the anchor group is the weak point and the π-interactions between the pyrene group and the MWCNT are not sufficiently strong to prevent desorption. Since catalysis was conducted at a potential that is less negative than the potential required for the reduction of pyrene,[14] *i.e.* at −2.20 V, we assume that it is related to the rather good solubility of the reduced catalyst in the solvent mixture rather than to the redox activity of the pyrene anchor.

Since the catalyst precursor **1** is not soluble in water, we investigated the hybrid in 100% water in order to prevent desorption. The current of **1**@MWCNT under $N_2$ atmosphere in water with 0.5 M $NaHCO_3$ as electrolyte is much larger than in dmf/water. The CV data do not show pronounced redox processes, and only one small, broad redox feature at $E_{p,c}$ of ~−1.03 V *vs.* SCE[13,15] was observed (Fig. S18†). The current quickly decreases with increasing number of cycles due to the decrease in the capacitive current (Fig. S18 and S22†), though in contrast to dmf/water the redox wave at −1.03 V, which we assigned to **1**, did not vanish. Under $CO_2$ atmosphere the current is larger than under $N_2$, which indicates some catalytic activity, though the current increase is less distinct than in dmf/water (Fig. S19†). The current decreases with the number of scans, and after ~15 cycles the current is similar to the current observed under $N_2$ (Fig. S20 and S21†). The current of bare MWCNT decreases slightly under $CO_2$ atmosphere (Fig. S22†). CPE experiments at −1.37 V *vs.* SCE confirmed the drop of the current within the first 100 s of the experiment (Fig. S26†). No CO was produced during the bulk electrolysis experiment, but instead $H_2$ was formed with a Faraday yield of about 20%. However, high resolution XPS after 30 minutes of electrolysis confirmed the presence of the catalyst on the electrode surface as the rhenium $4f^{7/2}$ and $4f^{5/2}$ peaks were still present (Fig. S34†). The binding energies are shifted to higher energies (42.1 and 44.5 eV), which indicates that the complex is not reduced, as this would lead to a shift to lower energies. This suggests that the lack of CO production in 0.5 M aqueous $NaHCO_3$ is not associated with catalyst desorption as in dmf/water. In the blank CPE experiment of a GC electrode just coated with MWCNT, the current also drops within the first minutes, however, it stabilises at a lower level than in the experiment of **1**@MWCNT. Though, $H_2$ was formed in a higher Faraday yield of about 64% (Table S4 and Fig. S27†). In both experiments the current drops, which we attributed to an increase of the pH near the electrode surface upon consumption of protons due to HER and a decrease in the capacitive current. However, solely $H_2$ is formed in both experiments, which indicates that the Re complex has virtually no influence on the product distribution. This could be rationalised by, *e.g.*, the differences in the proton (and $CO_2$) concentrations in dmf/water mixtures, which is basic (pH ~ 10) in comparison to water/$HCO_3^-$, which is less basic (pH ~ 8). Since the respective reaction rates depend on the proton and $CO_2$ concentrations, these differences could alter product formation and/or reduce the overpotential for $H^+$ reduction. In contrast to the work of Warren and co-workers on similar systems, **1** turned to an inactive catalyst in water upon heterogenisation, which supports their statement that medium effects can have an important impact on the activity.[8]

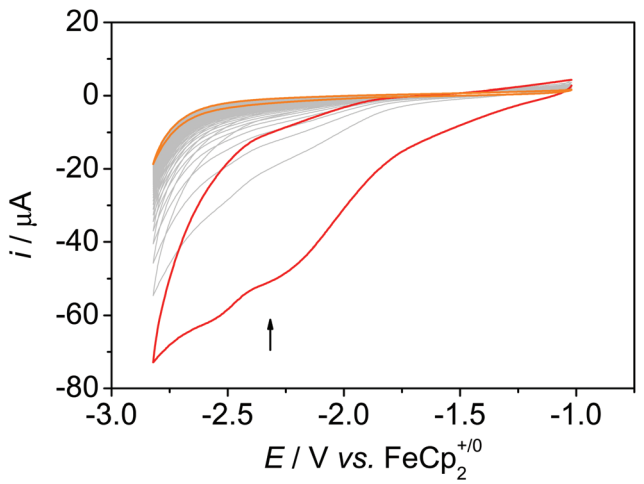


Fig. 6 50 CV scans of **1**@MWCNT under $CO_2$ atmosphere in dmf + 10% water, 0.1 M $^nBu_4NPF_6$, $\nu$ = 0.1 V s$^{-1}$.

## Conclusion

The dinuclear Re complex **1** is an active catalyst in the electrochemical syngas formation, that is it catalyses the $CO_2$-to-CO conversion and $H^+$-to-$H_2$ conversion in dmf/water with similar rates. Since the related complex **I** without a pyrene unit in con-

jugation to the proton responsive phenol unit catalyses selectively the CO formation, we assume that the differences in the thermodynamics of the phenol-pyrene *versus* the *tert*-butylphenol unit may give rise to the small differences in the reaction rates for $H_2$ formation. The complexes exhibit different H-donor properties, the acidity of the OH unit in **1** is larger than in **I**, and the redox activity of the pyrene unit may lead to changes in the BDFE of the OH unit. In other words, although, the electronic structure and the redox properties of the metal centre are virtually unaffected by the pyrene unit, the pyrene unit in the backbone has an influence on the reactivity. Immobilisation of the complex on MWCNT on a GC electrode was successful, however, the complex quickly desorbs under reductive conditions in dmf/water. Changing to 0.5 M aqueous $NaHCO_3$ as solvent leads to a loss of activity for $CO_2$-to-CO conversion and only $H_2$ formation was observed, as in the blank reaction. XPS confirmed a high stability of the complex on the electrode surface in 0.5 M aqueous $NaHCO_3$. This underscores that medium effects have a large impact on the catalytic activity.[23] The large differences in proton concentration in water and water/dmf mixtures may alter the reaction rates for $H_2$ and CO formation and/or lower the overpotential for $H_2$ evolution in water.

## Experimental section

ESI† includes experimental details for the ligand synthesis, all details on X-Ray crystallography, further electrochemical measurements, IR data, as well as SEM pictures and XPS data.

### General information

Manipulations of air-sensitive reagents were carried out by means of common Schlenk-type techniques involving the use of a dry argon or nitrogen atmosphere or performed in an MBraun glovebox. If not otherwise stated, the potentials in this paper are given *vs.* $Fc^{+/0}$ in organic solvents and *vs.* SCE in water. MWCNTs were purified according to a literature procedure prior to use.[24]

**Synthesis of 1.** **11** (33.0 mg, 54.2 μmol, 1.00 eq.) and $Re(CO)_5Cl$ (39.2 mg, 108 μmol, 1.99 eq.) were suspended in toluene (5 mL) and the suspension was stirred at 110 °C for six hours. After cooling to r.t. the precipitate was filtered off and washed with diethylether (3 × 2 mL) and hexane (3 × 2 mL). After drying *in vacuo* **1** was obtained as yellow solid in 65% yield. $^1$H-NMR (Fig. S35†) (300 MHz, dmso-$d_6$, ppm, major isomer): $\delta$ = 9.79 (s, OH, 1H), 8.74 (d, $J$ = 9.4 Hz, Pyr-CH, 1H), 8.41–8.23 (m, Ar–CH, 9H), 8.21–8.02 (m, Ar–CH, 5H), 7.69 (d, $^3J_{HH}$ = 1.1 Hz, Im–CH, 2H), 7.61 (s, Ar–CH, 2H), 7.50 (d, $^3J_{HH}$ = 1.4 Hz, 2H), 4.26 (s, $NCH_3$, 6H). $^1$H-NMR (300 MHz, dmso-$d_6$, ppm, minor isomer): $\delta$ = 9.17 (s, OH, 1H), 8.56 (d, $J$ = 9.1 Hz, Pyr–CH, 1H), 8.41–8.23 (m, Ar–CH, 9H), 8.21–8.02 (m, Ar–CH, 5H), 7.68–7.64 (m, Im–CH, 2H), 7.60–7.58 (m, Ar–CH, 2H), 7.49–7.46 (s, Im–CH, 2H), 4.22 (s, $NCH_3$, 6H). $^{13}$C-NMR (75 MHz, dmso-$d_6$, ppm, all isomers): $\delta$ = 197.5 (CO), 196.0 (CO), 189.5 (CO), 160.8, 151.1, 147.9, 147.0, 146.8, 140.1, 136.0, 134.2, 131.3, 131.0, 130.9, 130.5, 130.4, 129.9, 129.1, 128.9, 128.3, 128.2, 128.0, 127.9, 127.8, 127.7, 127.6, 127.4, 127.3, 127.2, 126.3, 126.3, 125.5, 125.4, 125.0, 125.0, 124.9, 124.7, 124.2, 124.0, 121.5, 36.7 ($NCH_3$). MS (ESI MeOH): $m/z$ = 1147.1014 $[M\text{-}H\text{-}2Cl]^+$. IR (KBr, $cm^{-1}$): 684 (w), 724 (w), 750 (w), 811 (m), 849 (m), 1090 (m), 1225 (w), 1259 (m), 1469 (m), 1503 (m), 1565 (w), 1610 (m), 1888 (s), 1901 (s), 2015 (s), 2925 (w), 2961 (w), 3045 (w), 3132 (w), 3153 (w), 3430 (m). $C_{46}H_{28}O_7N_6Re_2Cl_2$·dmf calcd: C: 45.4; H: 2.7; N: 7.6; found: C: 45.3; H: 3.0; N: 7.8.

**Preparation of 1@MWCNT.** The GC electrodes were coated with MWCNT by dip coating a suspension of MWCNT (35.4 μL $cm^{-2}$) in thf. This procedure was repeated nine times and the coated electrodes were dried *in vacuo*.

**1** was adsorbed by soaking MWCNT coated electrodes in a saturated solution of **1** in MeCN overnight. The soaked electrodes were rinsed with small amounts of fresh MeCN to remove unbound **1** and subsequently dried under a gentle nitrogen stream.

## Conflicts of interest

There are no conflicts to declare.

## Acknowledgements

This work was supported by funding from the DFG [SI 1577-2 (I. S.), SFB 1073 (I. S., F. M., C. J. project C01)], the Fonds der Chemischen Industrie, the Georg-August-Universität Göttingen, and the Otto-Röhm-Gedächtnisstiftung. We thank Dr C. Volkmann for measuring the X-Ray structure and Christian Höhn, Helmholtz-Zentrum Berlin für Materialien und Energie, for measuring the XPS. We thank Igor Fokin for conducting some CPE experiments. Support by Göttingen University is acknowledged.

## References

1 A. Tatin, J. Bonin and M. Robert, *ACS Energy Lett.*, 2016, **1**, 1062–1064; R. Foit, I. C. Vinke, L. G. J. de Haart and R. A. Eichel, *Angew. Chem., Int. Ed.*, 2017, **56**, 5402–5411.

2 M. L. Pegis, J. A. S. Roberts, D. J. Wasylenko, E. A. Mader, A. M. Appel and J. M. Mayer, *Inorg. Chem.*, 2015, **54**, 11883–11888.

3 J. Hawecker, J.-M. Lehn and R. Ziessel, *J. Chem. Soc., Chem. Commun.*, 1984, **984**, 328–330.

4 (*a*) B. P. Sullivan, C. M. Bolinger, D. Conrad, W. J. Vining and T. J. Meyer, *J. Chem. Soc., Chem. Commun.*, 1985, **985**, 1414–1416; (*b*) J. Hawecker, J.-M. Lehn and R. Ziessel, *Helv. Chim. Acta*, 1986, **69**, 1990–2012; (*c*) T. R. O'Toole, B. P. Sullivan, M. R.-M. Bruce, L. D. Margerum, R. W. Murray and T. J. Meyer, *J. Electroanal. Chem. Interfacial Electrochem.*, 1989, **259**, 217–239; (*d*) Y. Hayashi, S. Kita, B. S. Brunschwig and E. Fujita, *J. Am. Chem. Soc.*, 2003, **125**,

11976–11987; (*e*) A. J. Morris, G. J. Meyer and E. Fujita, *Acc. Chem. Res.*, 2009, **42**, 1983–1994; (*f*) J. Agarwal, E. Fujita, H. F. Schaefer 3rd and J. T. Muckerman, *J. Am. Chem. Soc.*, 2012, **134**, 5180–5186; (*g*) J. A. Keith, K. A. Grice, C. P. Kubiak and E. A. Carter, *J. Am. Chem. Soc.*, 2013, **135**, 15823–15829; and references therein.

5 (*a*) G. F. Manbeck, J. T. Muckerman, D. J. Szalda, Y. Himeda and E. Fujita, *J. Phys. Chem. B*, 2015, **119**, 7457–7466; (*b*) A. Wilting, T. Stolper, R. A. Mata and I. Siewert, *Inorg. Chem.*, 2017, **56**, 4176–4185; (*c*) A. Wilting and I. Siewert, *ChemistrySelect*, 2018, **3**, 4593–4597; (*d*) J.-P. Du, A. Wilting and I. Siewert, *Chem. – Eur. J.*, 2019, **25**, 5555–5564; (*e*) L. Rotundo, C. Garino, E. Priola, D. Sassone, H. Rao, B. Ma, M. Robert, J. Fiedler, R. Gobetto and C. Nervi, *Organometallics*, 2019, **38**, 1351–1360; (*f*) S. A. Roell, B. R. Schrage, C. J. Ziegler and T. A. White, *Inorg. Chim. Acta*, 2020, **503**, 119397; (*g*) J. O. Taylor, G. Neri, L. Banerji, A. J. Cowan and F. Hartl, *Inorg. Chem.*, 2020, **59**, 5564–5578.

6 C. Sun, S. Prosperini, P. Quagliotto, G. Viscardi, S. S. Yoon, R. Gobetto and C. Nervi, *Dalton Trans.*, 2016, **45**, 14678–14688.

7 J. D. Blakemore, A. Gupta, J. J. Warren, B. S. Brunschwig and H. B. Gray, *J. Am. Chem. Soc.*, 2013, **135**, 18288–18291.

8 S. Sinha, A. Sonea, W. Shen, S. S. Hanson and J. J. Warren, *Inorg. Chem.*, 2019, **58**, 10454–10461.

9 A. Zhanaidarova, S. C. Jones, E. Despagnet-Ayoub, B. R. Pimentel and C. P. Kubiak, *J. Am. Chem. Soc.*, 2019, **141**, 17270–17277.

10 A. Wilting, M. Kügler and I. Siewert, *Z. Anorg. Allg. Chem.*, 2015, **641**, 2498–2505.

11 F. A. Cotton and C. S. Kraihanzel, *J. Am. Chem. Soc.*, 1962, **84**, 4432–4438.

12 C. A. Hunter and J. K. M. Sanders, *J. Am. Chem. Soc.*, 1990, **112**, 5525–5534.

13 I. M. Kolthoff, M. K. Chantooni, *et al.*, report a slightly different value of −0.69 V for the $H^+|H_2$ redox couple *vs.* $Fc^{+/0}$ in dmf. $Fc^{+/0}$ exhibits a standard reduction potential of 0.40 V *vs.* $H^+|H_2$ in water, *J. Phys. Chem.*, 1972, **76**, 2024–2034.

14 M.-A. Tehfe, J. Lalevée, F. Morlet-Savary, B. Graff, N. Blanchard and J.-P. Fouassier, *Macromolecules*, 2012, **45**, 1746–1752.

15 For the conversion of the potential from $Fc^{+/0}$ to SCE see: N. G. Connelly and W. E. Geiger, *Chem. Rev.*, 1996, **96**, 877–910.

16 J. M. Smieja and C. P. Kubiak, *Inorg. Chem.*, 2010, **49**, 9283–9289.

17 B. Bernet and A. Vasella, *Helv. Chim. Acta*, 2000, **83**, 995–1021.

18 J. J. Warren, T. A. Tronic and J. M. Mayer, *Chem. Rev.*, 2010, **110**, 6961–7001.

19 J. M. Saveant and E. Vianello, *Electrochim. Acta*, 1965, **10**, 905–920.

20 A. J. Bard and L. R. Faulkner, *Electrochemical Methods: Fundamentals and Applications*, Wiley, New York, 2nd edn, 2001.

21 A. M. Appel and M. L. Helm, *ACS Catal.*, 2014, **4**, 630–633.

22 S. Sinha and J. J. Warren, *Inorg. Chem.*, 2018, **57**, 12650–12656.

23 G. Gritzner, *J. Electroanal. Chem. Interfacial Electrochem.*, 1983, **144**, 259–277; M. J. Kamlet, J. L. M. Abboud, M. H. Abraham and R. W. Taft, *J. Org. Chem.*, 1983, **48**, 2877–2887; D. Acevedo and H. D. Abruna, *J. Phys. Chem.*, 1991, **95**, 9590–9594; H. Svith, H. Jensen, J. Almstedt, P. Andersson, T. Lundbäck, K. Daasbjerg and M. Jonsson, *J. Phys. Chem. A*, 2004, **108**, 4805–4811.

24 A. Ali Moosa, M. Ibrahim and R. F. Salloom, *Int. J. Nano Dimens.*, 2014, **5**, 97–104.